Supplementary Information for Publication

Geometric notch-manipulated skyrmion dynamics for reconfigurable diode and logic gates in synthetic antiferromagnetic nanotrack†

Min Fan,[‡a] Min Xu,[‡*a] Changping Xu,[a] Changjing Hu,[a] Haihong Tang,[a] Hehang Zhang[a] and Zhiyu Zhang[b]

[a]*Key Laboratory for Anisotropy and Texture of Materials (MOE), School of Materials Science and Engineering, Northeastern University, Shenyang, 110819, China. Email: xum@mail.neu.edu.cn*

[b]*School of Physics, State Key Laboratory for Crystal Materials, Shandong University, Jinan 250100, China*

†Electronic supplementary information (ESI) available.

‡These authors contributed equally to this work.

*Corresponding author. E-mail: xum@mail.neu.edu.cn

SI1. Dynamics explanation of skyrmion's velocity variation with position

During the skyrmion's forward passage through the notch region, its velocity exhibits a characteristic "W"-shaped variation with position, as shown in Fig. 2(a), which can be explained by the established dynamic equations and the energy potential barrier induced by the geometric structure. Upon entering the trapezoidal notch channel, from eqn (5), the skyrmion velocity $\left(\frac{\sigma\kappa j_{\mathrm{CH}}\cos\theta}{\alpha \mathrm{D}}\right)$ is lower than that in the initial stage due to the tilt angle θ of the trapezoidal notch. During this entry, the skyrmion is subjected not only to the dissipative force as resistance but also to the repulsive force from the inclined edge of the notch, leading to a sharp decline in velocity. Additionally, the tilt angle of the notch's inclined side narrows the effective channel upon entry, which

creates a constriction region that the skyrmion enters. In this region, the geometric constraint increases motion resistance and converts kinetic energy into potential energy of magnetic moment distortion, ultimately resulting in a minimum in the skyrmion velocity. On entering the parallel narrow channel within the notch, the skyrmion velocity rebounds from eqn (5). At this point, the repulsive force from the inclined edge of the notch vanishes, which enables the driving force from SOT to dominate and thereby accelerate the skyrmion. The geometry inside the trapezoidal notch channel corresponds to a "valley" in the potential energy distribution; thus, as the skyrmion enters the channel interior along the high-potential inclined edge of the notch, the potential energy is converted into kinetic energy, causing its velocity to rise to a maximum. When exiting the trapezoidal notch and approaching the triangular notch channel, the skyrmion decelerates due to the tilt angle θ' of the triangular notch's hypotenuse. Concurrently, the structural discontinuity encountered by the skyrmion causes a surge in its motional resistance, driving its velocity to drop to a minimum again. As the skyrmion penetrates further, the perpendicular edge of the trapezoidal notch exerts a repulsive force that promotes its motion along the $+x$ direction, and combined with the widening of the narrow channel, this leads to another rebound in its velocity. After the skyrmion breaks away from the notch channel, the SOT driving force and the dissipative force reach dynamic equilibrium again, resulting in the rapid recovery of the skyrmion's kinetic energy and the restoration of its velocity to the initial state $\left(\frac{\sigma\kappa j_{\mathrm{CH}}}{\alpha \mathsf{D}}\right)$.

SI2. Magnetization reversal to achieve NOT, NAND, and NOR functions

The reversal of magnetization can be triggered by a sufficiently strong spin-orbit torque generated via the in-plane current, which can be achieved by incorporating the exchange bias from the antiferromagnetic top layer. Thus, the magnetization orientation of the ferromagnetic layer can be controlled by the in-plane current. Under this mechanism, when no skyrmion is generated at either of the two input terminals (MTJ-

1 and MTJ-2), the input is recorded as "0"; in this scenario, no skyrmion reaches the output terminal (MTJ-3), and the output is inverted to "1", while when a skyrmion is generated at either input terminal, the input switches to "1", and upon the arrival of this skyrmion at the output terminal, the output is inverted to "0". This mechanism can thus implement the NOT logic operation. Analogously, by reversing the magnetization orientation of the ferromagnetic layer at the output terminal, the NAND and NOR logic functions can be implemented based on the existing AND and OR architectures, thereby achieving logic reconfigurability.

SI3. Influence of geometric parameters *h* and *d* on skyrmion velocity

As detailed in our model and method, in the proposed reconfigurable synthetic antiferromagnetic (SAF) nanotrack structure with asymmetric geometric notches featuring tilted edges, there are two key geometric parameters: the distance between the shorter base of the trapezoidal notch and the lower boundary of the nanotrack is denoted as h, and the distance between the perpendicular sides of the trapezoidal and triangular notches is denoted as d. To further elucidate the influence of the geometric structure parameters on skyrmion dynamics, we have investigated the velocity of a single skyrmion traversing the notch channel region as a function of d or h, under the condition that the tilt angles (θ and θ') of the tilted edges of the right trapezoidal notch and right triangular notch remain constant, as illustrated in Fig. S1. Herein, θ and θ' are fixed at 45°, angles at which the proposed device can achieve reconfigurable diode and logic gate functions. It is found that when h is fixed, the velocity of the skyrmion passing through the triangular notch channel region increases with increasing d, while when d is fixed, the velocity of the skyrmion traversing the notch channel region increases as h increases. This behavior is attributed to the geometric confinement effect: a larger value of either h or d, more precisely, a larger d (for fixed h) or a larger h (for fixed d), corresponds to a wider notch channel region, which in turn lowers the potential energy barrier induced by the notches. Consequently, the skyrmion encounters less resistance, which enables it to pass through the notch channel region at a higher velocity.

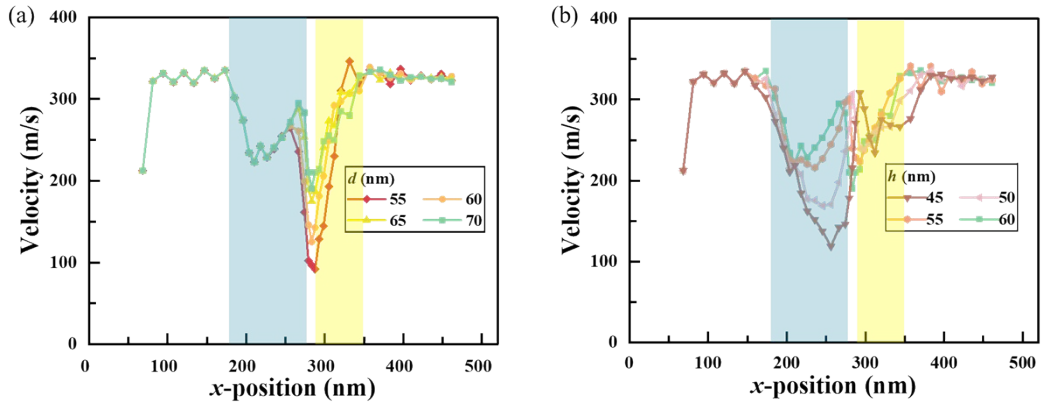

Fig. S1 (a) Velocity of a single skyrmion when passing forward through the geometric notch channel region as a function of d values when h is fixed. (b) Velocity of a single skyrmion when passing forward through the notch channel region as a function h values when d is fixed. (Both θ and θ' are 45°.)

SI4. Effect of damping constants on skyrmion velocity

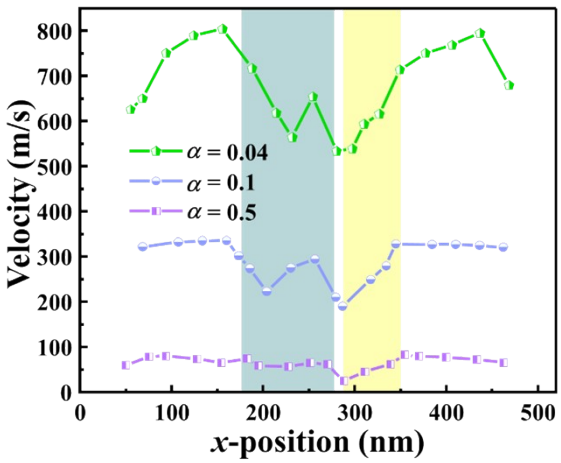

Fig. S2 Effect of different damping constants α on skyrmion velocity (d=60 nm; h = 70 nm; $\theta = \theta' = 45°$).

Based on the analysis of skyrmion dynamics for different damping constant α values, Fig. S2 demonstrates the effect of different α values on skyrmion velocity. By comparing the skyrmion velocity changes at different α values, it is found that as α increases, the skyrmion velocity decreases significantly. This phenomenon aligns with

theoretical expectations, as higher damping constants enhance energy dissipation, leading to a reduction in skyrmion velocity. In this study, the damping constant α is an important parameter influencing skyrmion motion, particularly in synthetic antiferromagnetic (SAF) nanotracks. When the α value is higher, the skyrmion dynamics become slower, which means that a reasonable selection of α needs to be made in the design to balance device speed and power consumption. Therefore, this figure effectively illustrates the impact of different α values on skyrmion motion, providing further theoretical support for the proposed device design, especially in terms of how to optimize the damping constant for the best performance when considering reconfigurable functionality and low-power applications.

SI5. Variation of skyrmion velocity components as a function of current density

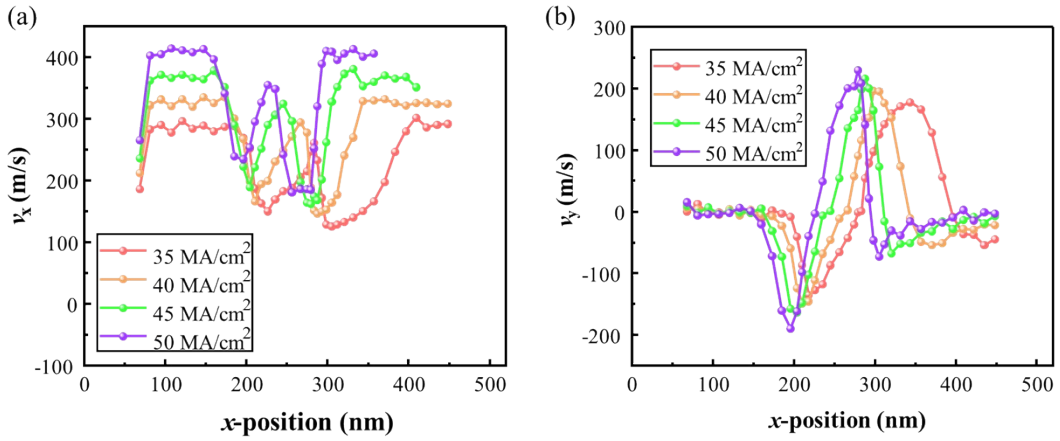

Fig. S3 Variation of the skyrmion velocity components as a function of current density. (a) Variation of the skyrmion horizontal velocity component v_x as a function of current density. (b) Variation of the skyrmion vertical velocity component v_y as a function of current density. (d=60 nm; h = 70 nm; $\theta = \theta' = 45°$)

Variation of the skyrmion velocity components as a function of current density is shown in Fig. S3. In the trapezoidal notch region (represented by the blue energy barrier in Fig. 2(c)), skyrmions encounter a significant energy barrier that causes strong geometric constraints on their motion. At this point, the skyrmions must overcome the energy

obstacle created by the boundary, which leads to a reduction in both the horizontal velocity (v_x) and vertical velocity (v_y). This slowdown is primarily due to the non-uniform energy barrier induced by the geometry of the trapezoidal notch, which restricts skyrmion motion in this region.

Unlike the trapezoidal notch, the geometry of the triangular notch region (represented by the yellow energy barrier) results in different effects on the skyrmion's horizontal and vertical velocities. The sharp boundary of the triangular notch causes the skyrmion's speed to vary significantly as it passes through this region. At higher current densities, skyrmions can move at higher speeds through the triangular notch; however, at lower current densities, their speed is reduced due to interactions with the notch boundaries.

The v_x component represents the skyrmion's horizontal velocity. In the trapezoidal notch region, due to the strong geometric constraints, v_x decreases significantly, which leads to a reduction in total velocity v (shown in Fig. 2(c)). In the triangular notch region, although v_x recovers to some extent, it still experiences some influence from the geometric constraints, resulting in a more gradual increase in total velocity. Overall, total velocity v reflects the combined effect of v_x and v_y, with v_x having a more significant influence on total velocity in some regions. The v_y component represents the skyrmion's vertical velocity. In the trapezoidal notch region, the vertical velocity v_y is significantly suppressed, leading to lower v_y values. In the triangular notch region, due to the different geometry, v_y shows more significant variation, especially at higher current densities, where v_y increases substantially, showing a clear acceleration trend. Although v_y contributes less to total velocity compared to v_x, its effect cannot be ignored in certain regions, particularly in the triangular notch region.

The total velocity v is the combined effect of v_x and v_y. As shown in Fig. 2(c), total velocity increases with increasing current density. At low current densities, the skyrmion's motion is primarily constrained by the geometry of both the trapezoidal and triangular notches, leading to a lower total velocity v. As the current density increases, the skyrmion is able to overcome these constraints, and total velocity v increases significantly, especially in the triangular notch region, where skyrmion acceleration is more pronounced.

From the above analysis, it can be seen that skyrmion motion is influenced not only by current density but also by the geometry of the notches. The trapezoidal and triangular notches have different effects on v_x and v_y, which in turn impact the total velocity v. In the trapezoidal notch region, both horizontal and vertical velocities are strongly constrained, while in the triangular notch region, the skyrmion speeds recover more quickly, particularly at higher current densities. This detailed analysis provides a clearer understanding of the relationship between v_x, v_y, and total velocity, as well as how the notch geometry influences skyrmion dynamics.

SI6. Influence of thermal perturbations on reconfigurable functions

We have investigated how thermal perturbations induced by finite temperatures affect reconfigurable logic and diode functions based on skyrmions. When the temperature is increased to 120 K, the influence of thermal perturbations on the reconfigurable functions of skyrmions is shown in Fig. S4. It is found that thermal perturbations induced by temperature lead to the deformation of skyrmions; however, the deformed skyrmions can still execute the AND logic function under spin-current driving, as shown in Fig. S4(a), and the OR logic function, as presented in Fig. S4(b) and (c). In addition, the unidirectional transmission function of the skyrmion diode can also be realized at this temperature, as depicted in Fig. S4(c) and (d), where the skyrmion moving in the reverse direction is pinned by the triangular notch. The effect of thermal perturbations on the dynamics of skyrmions moving in the synthetic antiferromagnetic nanotrack manipulated by geometric notches demonstrates that such skyrmion-based reconfigurable device exhibit excellent robustness and application potential at finite temperatures.

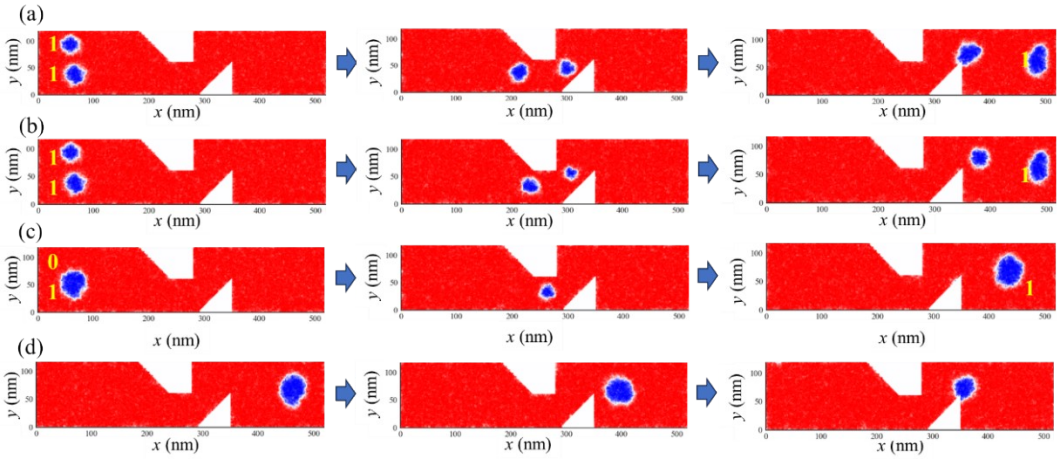

Fig. S4 Effect of thermal perturbations at 120 K on skyrmion-based logic and diode functions (h = 60 nm, d = 70 nm, $\theta = \theta' = 45°$). (a) Implementation of AND logic ("1 · 1 = 1") at a current density of 48 MA/cm². (b) Implementation of OR logic ("1 + 1 = 1") at 50 MA/cm². (c) Implementation of OR logic ("0 + 1 = 1") or diode forward conduction via skyrmion forward passage at 50 MA/cm². (d) Implementation of diode reverse blocking via skyrmion pinning during reverse motion at 50 MA/cm².

SI7. Energy consumption estimation for the reconfigurable device

In practical applications, the energy consumption of spintronic devices is a crucial performance indicator. For the proposed skyrmion-based device, the total energy consumption is the sum of the energies required for writing, manipulating, and detecting skyrmions: $E = E_{\text{write}} + E_{\text{manipulate}} + E_{\text{detect}}$, where E_{write} and E_{detect} represent the energy consumption for the creation and detection of the skyrmion at the writing and reading terminals of the magnetic tunnel junction (MTJ), respectively. For a single skyrmion, these two parts of energy consumption are approximately 3.1 fJ and 0.8 fJ, respectively. The energy consumption of the skyrmion during the driving process, as shown below, mainly depends on the Joule heat generated within the heavy metal (HM) layer (Pt layer) to which an in-plane current is applied.

$$E_{\text{manipulate}} = I^2 R_{\text{HM}} \Delta t = \rho_{\text{HM}} d_{\text{HM}} j^2 S \Delta t$$

where I represents the current, and R_{HM} denotes the resistance of the heavy metal layer.

$R_{HM} = \rho_{HM} d_{HM} j^2 S$, where j represents the current density, and the resistivity ρ_{HM}, thickness d_{HM}, and surface area S of the Pt layer are 106 nΩ·m, 2 nm and 520×120 nm^2, respectively. In this study, when the device functions as a diode, MTJ-1 and MTJ-3 serve as the writing and reading terminals, respectively. For example, when d, h, θ, and θ' are 70 nm, 60 nm, 45°, and 45°, respectively (These geometric dimensions are shown in Fig. 1), the total energy consumption of the diode device for this unidirectional transport system ranges from 4.89 fJ to 8.55 fJ. When j is the minimum threshold current density (10 mA/cm^2), the minimum energy consumption for achieving diode functionality is as low as 4.89 fJ. Under the same device dimensions, when the device functions as a logic gate, its energy consumption can be divided into two cases. When performing single skyrmion logic, its writing and reading terminals are the same as those of the diode, and its energy consumption is also the same as that of the diode's unidirectional transport. When performing dual skyrmion logic, MTJ-1 and MTJ-2 serve as writing terminals, while MTJ-3 acts as the detecting terminal. For this system, when implementing AND logic, under a driving current of 7.5 mA/cm^2, the minimum total energy consumption of the logic device is approximately 8.46 fJ, while when implementing OR logic, under a driving current of 8 mA/cm^2, the minimum total energy consumption is approximately 8.56 fJ. It is concluded that the energy consumption of the reconfigurable diode and logic device demonstrates a significant advantage over CMOS diodes and logic gates.

References

1. M. Song, M. G. Park, S. Ko, S. K. Jang, M. Je and K. J. Kim, *IEEE Trans. Electron Devices*, 2021, **68**, 1939-1943.
2. R. Tomasello, K. Y. Guslienko, M. Ricci, A. Giordano, J. Barker, M. Carpentieri, O. Chubykalo-Fesenko and G. Finocchio, *Phys. Rev. B*, 2018, **97**, 060402.
3. M. G. Mankalale, Z. Zhao, J. P. Wang and S. S. Sapatnekar, *IEEE Trans. Electron Devices*, 2019, **66**, 1990-1996.
4. Y. Chen and X. Xing, *IEEE Trans. Magn.*, 2024, **60**, 1-6.